I. IONIZATION COOLING

A. Introduction

The muon beam at the end of the decay channel is very intense, but diffuse in phase space. For a high luminosity collider, the phase-space volume of the muon beam must be reduced within a time of the order of the μ lifetime $\approx 2\ \mu s$. This requires the development of a new method for beam cooling.

Cooling by synchrotron radiation, conventional stochastic cooling and conventional electron cooling are all too slow. Optical stochastic cooling [1], electron cooling in a plasma discharge [2] and cooling in a crystal lattice [3,4] are being studied, but appear technologically difficult. Ionization cooling [5–7] of muons seems relatively straightforward, and it is unique for muons.

Ionization cooling involves passing the beam through some material in which the muons lose both transverse and longitudinal momentum by ionization loss (dE/dx). The longitudinal muon momentum is then restored by reacceleration, leaving a net loss of transverse momentum (transverse cooling). The process is repeated many times to achieve a large cooling factor.

The energy spread can also be reduced (longitudinal emittance exchange) by introducing a transverse variation in the absorber density or thickness (e.g. a wedge) at a location where there is dispersion (the position is energy dependent). This method results in an a corresponding increase of transverse momentum and is thus not true cooling, but an exchange of longitudinal and transverse emittances that, with transverse cooling, allows cooling in all dimensions.

The appropriate figure of merit for cooling is the final value of the 6-D relativistically invariant emittance ϵ_6 – the area in the 6-dimensional phase space (x, y, z, p_x, p_y, p_z)– since, to a fairly good approximation, it is preserved during acceleration and storage in the collider ring. Theoretical studies have shown that, assuming realistic parameters for the cooling hardware, ionization cooling can be expected to reduce the phase-space volume occupied by the initial muon beam by a factor of $10^5 - 10^6$. A complete cooling channel would consist of $20 - 30$ cooling stages, each stage yielding about a factor of two in phase-space reduction.

It is recognized that the feasibility of constructing a muon ionization cooling channel is on the critical path to understanding the viability of the whole muon collider concept. The muon cooling channel is the most novel part of a muon collider complex. Steady progress has been made both in improving the design of the channel and in adding detail to the computer simulations. We are now close to the goal of having a detailed and complete simulation of an entire cooling channel. A vigorous experimental program is needed to verify and benchmark the computer simulations.

In the following parts of this section we will briefly describe the physics underlying the process of ionization cooling, we will show results of simulations for some chosen examples and mention a six year R&D program to demonstrate the feasibility of using ionization cooling techniques to reduce the 6-dimensional phase space emittance.

B. Cooling Theory

In ionization cooling, the beam loses both transverse and longitudinal momentum as it passes through a material medium. At the same time its emittance is increased due to stochastic multiple scattering and Landau straggling. Subsequently, the longitudinal momentum can be restored by reacceleration, leaving a net loss of transverse momentum.

The approximate equation for transverse cooling (with energies in GeV) is

$$\frac{d\epsilon_n}{ds} = -\frac{1}{\beta^2}\frac{dE_\mu}{ds}\ \frac{\epsilon_n}{E_\mu} + \frac{\beta_\perp (0.014)^2}{2\beta^3 E_\mu m_\mu\ L_R}, \tag{1}$$

where ϵ_n is the normalized transverse emittance, $\beta_\perp$ is the betatron function at the absorber, dE_μ/ds is the energy loss, and L_R is the radiation length of the material. The first term in this equation is the cooling term, and the second is the heating due to multiple scattering. This heating term is minimized if $\beta_\perp$ is small (strong-focusing) and L_R is large (a low-Z absorber).

The equation for energy spread (longitudinal emittance) is:

$$\frac{d(\Delta E)^2}{ds} = -2\ \frac{d\left(\frac{dE_\mu}{ds}\right)}{dE_\mu} < (\Delta E_\mu)^2 > + \frac{d(\Delta E_\mu)^2_{\text{straggling}}}{ds} \tag{2}$$

where the first term is the cooling (or heating) due to energy loss, and the second term is the heating due to straggling.

Energy spread can be reduced by artificially increasing $\frac{d(dE_\mu/ds)}{dE_\mu}$ by placing a transverse variation in absorber density or thickness at a location where position is energy dependent, i.e. where there is dispersion. The use of such wedges can reduce energy spread, but it simultaneously increases transverse emittance in the direction of the dispersion. Six dimensional phase space is not reduced, we only exchange longitudinal phase space with transverse phase space.

Ionization cooling of muons seems relatively straightforward in theory, but will require extensive simulation studies and hardware development for its optimization. There are practical problems in designing lattices that can transport, and focus the large emittance beam. There will also be effects from space charge and wake fields.

We have developed a number of tools for studying the ionization cooling process. First, the basic theory was used to identify the most promising beam properties, material type and focusing arrangements for cooling. Given the practical limits on magnetic field strengths, this gives an estimate of the minimum achievable emittance for a given configuration. Next, the differential equations for cooling and heating described above have been incorporated into a computer code. Allowance for the shifts in the betatron phase advance due to space charge and aberrations was included. This code was used to develop an overall cooling scenario, which broke the cooling system into a number of stages, and determined the properties of the beam, rf, and focusing lattice at each stage [8].

Finally, several tracking codes were either written or modified to study the cooling process in detail. Two new codes (SIMUCOOL [9], and ICOOL [10]) use Monte Carlo techniques to track particles one at a time through the cooling system. All the codes attempt to include all relevant physical processes to some degree, e.g. energy loss, straggling, multiple scattering, and to use Maxwellian models of the focusing fields. They do not yet take into account any space charge or wake field effects. In addition, we have also used a modified version of PARMELA [11] for tracking, which does include space charge effects, and a version of GEANT [12,13] that has been changed to double precision. All of these codes are continually being updated and optimized for studying the cooling problem.

C. Cooling System

The cooling is obtained in a series of cooling stages. Each stage consists of a succession of two components:

1. Transverse Cooling sections using materials in a strong focusing (low$\beta_\perp$) environments alternated with linac accelerators.

2. Emittance Exchange in lattices that generate dispersion, with absorbing material wedges to interchange reduce momentum spread.

In the examples that follow it is seen that each such stage lowers the 6 dimensional emittance by a factor of about 2. Since the required total 6 dimensional cooling is about 10^6, about 20 such stages are required. The total length of the system would be of the order of 500 m, and the total acceleration would be approximately 6 GeV. The fraction of muons remaining at the end of the cooling system is estimated to be $\approx 60\%$.

The baseline solution for transverse cooling involves the use of liquid hydrogen absorbers in strong solenoid focusing fields, interleaved with short linac sections. The solenoidal fields in successive absorbers is reversed to avoid build up of the canonical angular momentum. The focusing magnetic fields are not large (≈ 1 T) in the early stages where the emittances are large, but must increase as the emittance falls.

Two transverse cooling examples have been designed and simulated. The first would lie toward the end of a full cooling sequence and uses 15 T solenoids. The second, using 31 T solenoids, meets the requirements for the Higgs factory and could be the final cooling stage for this machine.

The baseline solution for emittance exchange involves the use of bent solenoids to generate dispersion and wedges of hydrogen or LiH to reduce the energy spread. A simulated example is given for exchange that would be needed after the 15 T transverse cooling case.

A lithium lens solution may prove more economical for the final stages, and might allow even lower emittances to be obtained. In this case, the lithium lens serves simultaneously to maintain the low $\beta_\perp$, and attenuate the beam momenta. Similar lenses, with surface fields of 10 T, were developed at Novosibirsk (BINP) and have been used, at low repetition rates, as focusing elements at FNAL and CERN [14–18]. Lenses for the cooling application, which would operate at 15 Hz, would need to employ flowing liquid lithium to provide adequate cooling. Higher surface fields would also be desirable.

Studies [19] have simulated cooling in multiple lithium lenses, and have shown cooling through several orders of magnitude. But these studies have, so far, used ideal matching and acceleration. Further studies are underway.

Cooling in beam recirculators could lead to reduction of costs of the cooling section [20], but again, full simulations with all higher order effects have not yet been successfully achieved.

D. 15 T Solenoid Transverse Cooling Example

The lattice consists of 11 identical 2 m long ‘cells’. In each cell there is a liquid hydrogen absorber (64 cm long, 10 cm diameter) in the 15 T solenoid focusing magnet (64 cm long, 12 cm diameter). The direction of the fields in the magnets alternates from one cell to the next. Between the magnets there are magnetic matching sections (1.3 m long, 32 cm inside diameter) where the field is lowered and then reversed. Inside the matching sections are short 805 MHz high gradient (36 MeV/m) linacs. Figure 1 shows the cross section of one cell of such a system, together with the beta function, and the magnetic field along the axis.

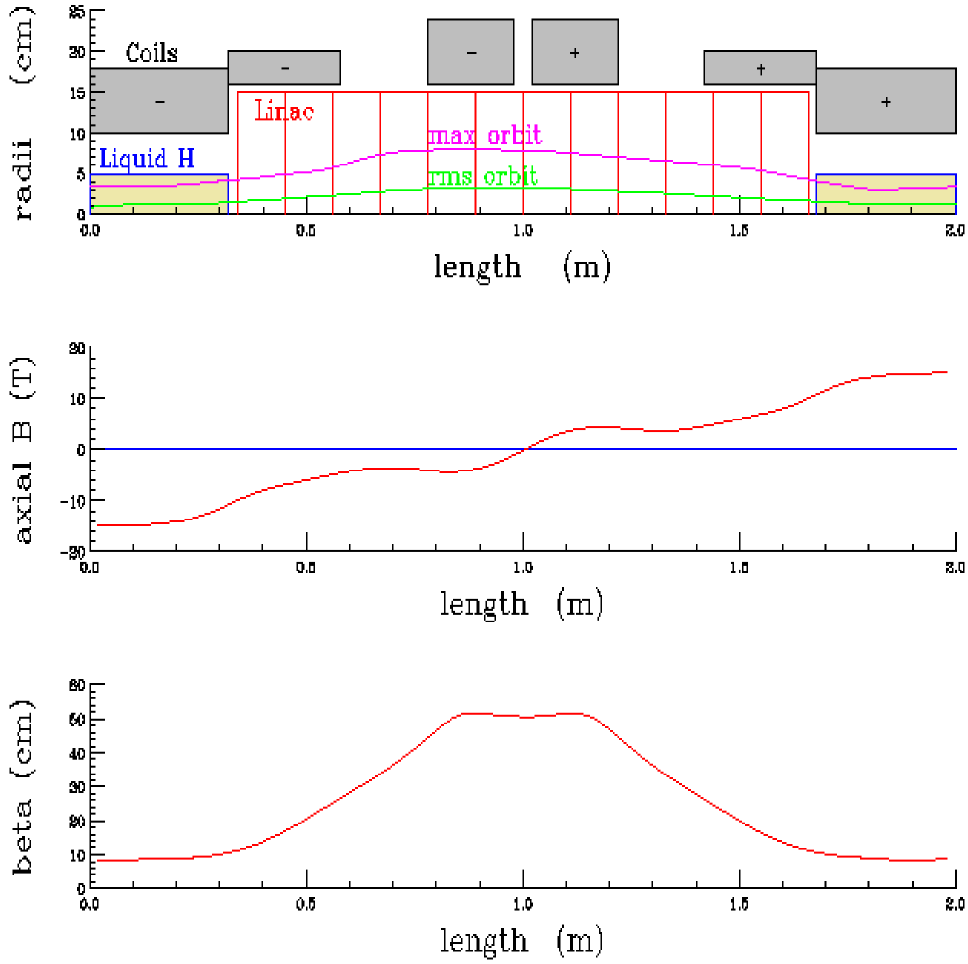

FIG. 1. a) Cross section of one cell of an alternating solenoid cooling system; b) axial magnetic field *vs.* z; c) beta function *vs.* z.

The simulations were performed using the program ICOOL [10]; the only effects which are not yet included are space charge and wake fields. Analytic vacuum calculations indicate that these effects should, for the later stages be significant, but not overwhelming, but a correct simulation must be done before we are assured that no significant problems exist. Particles are introduced with transverse and longitudinal emittance (186 MeV/c, 1400 π mm mrad transverse, and 1000 π mm δp/p longitudinal), together with a number of naturally occuring correlations: 1) the angular momentum appropriate for the starting axial magnetic field, 2) a correlation between momentum and amplitude squared to give forward velocities independent of amplitude, and 3) a distortion of the longitudinal bunch distribution to reflect the asymmetric nature of the alpha rf bucket.

Figure 2(a) shows the average momentum of the beam as it falls in the hydrogen absorbers and rises in the linacs. Figure 2(b) shows the average angular momentum, and (dashed) the canonical angular momentum, as they oscillate between positive and negative values in the reversing axial fields.

Figure 3(a) shows the rms and maximum radii of the beam as they rise and fall in the varying axial magnetic fields. Figure 3(b) shows the rms momentum corrected for the amplitude-momentum correlation. Figure 3(c) shows the rms bunch length.

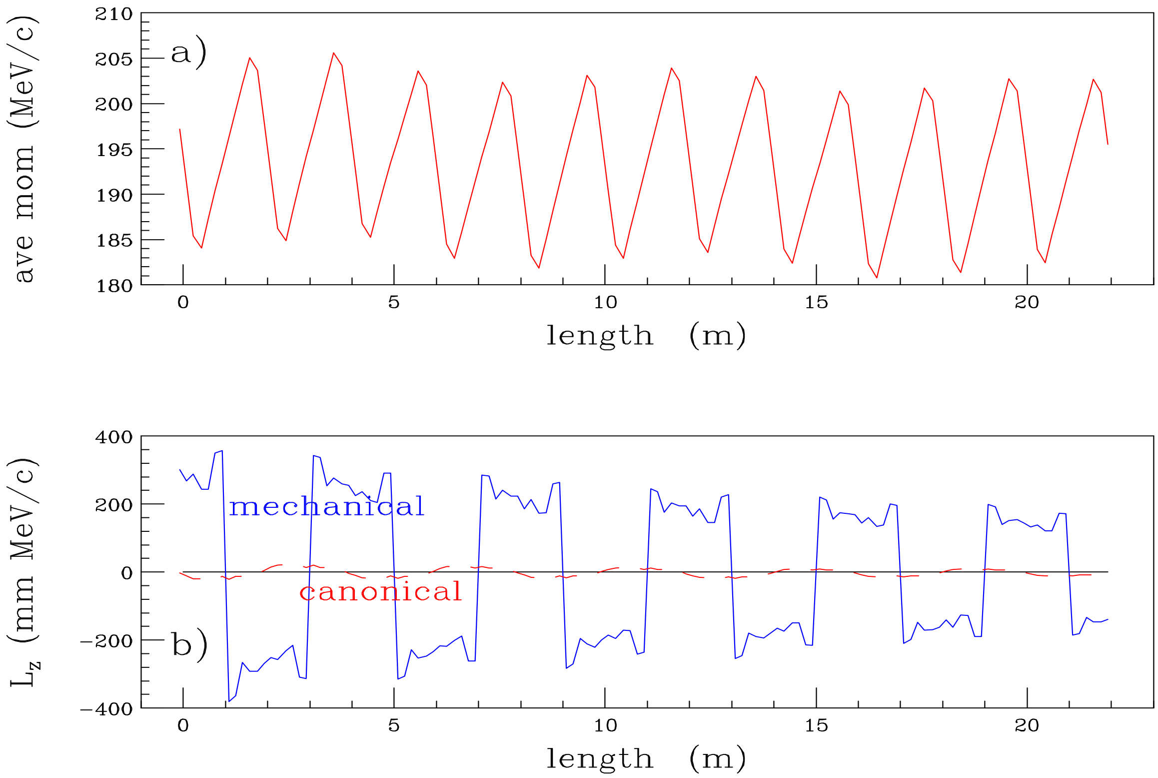

FIG. 2. a) average momentum vs. length; b) average angular momentum: true (solid curve) and canonical (dashed curve), vs. length.

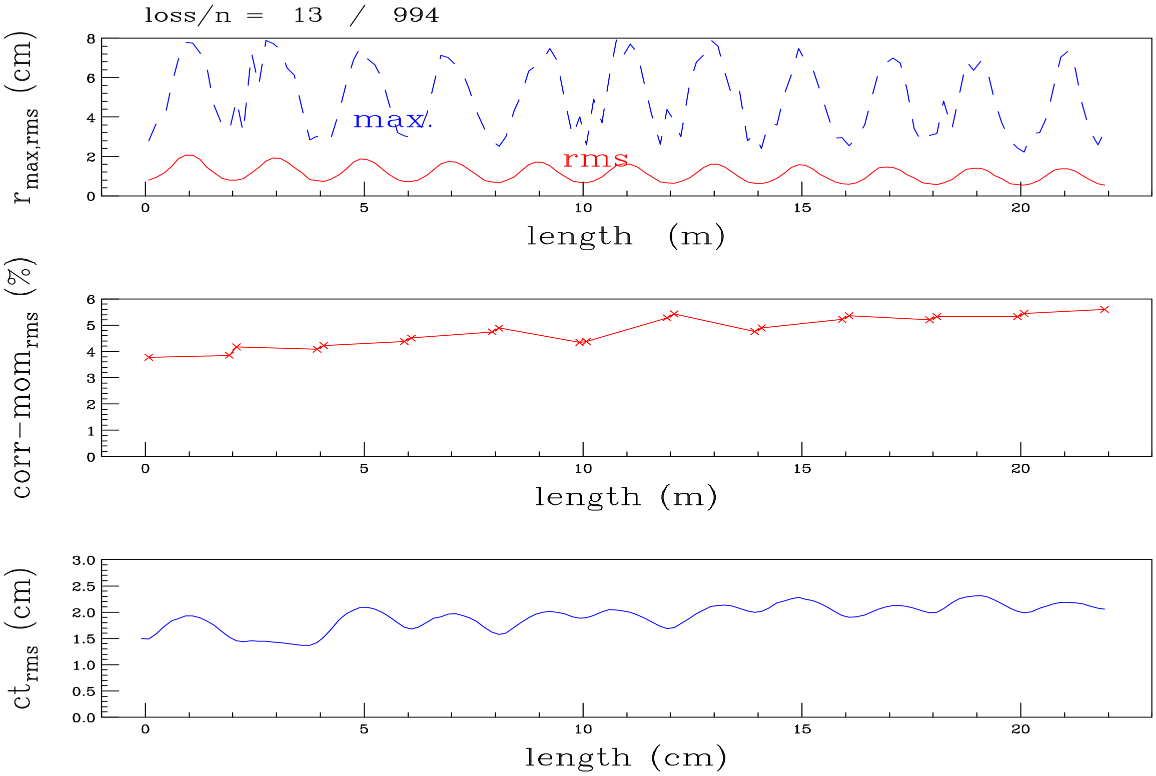

FIG. 3. a) rms and maximum beam radii, b) rms corrected momentum, c) rms bunch length; all vs. length.

Figure 4(a) shows the reduction of transverse emittance; Figure 4(b) shows the increase in longitudinal emittance induced by straggling and the adverse dependence of dE/dx with energy; Figure 4(c) shows the overall reduction in 6-dimensional emittance. Table I gives the initial and final parameters.

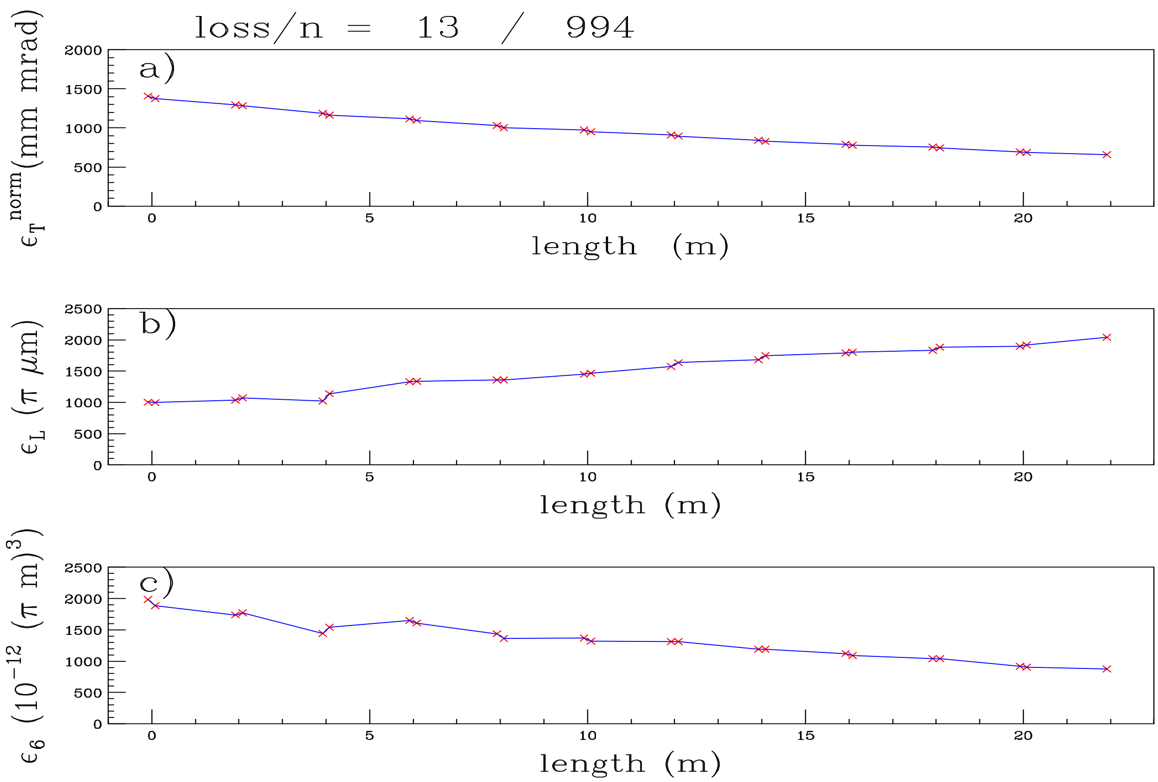

FIG. 4. emittance vs. length:a) transverse emittance; b)longitudinal emittance; and c) 6-dimensional emittance.

TABLE I. Initial and final beam parameters in a 15 T transverse cooling section.

		initial	final	factor
Particles tracked		1000	980	98%
Transverse Emittance	π mm mrad	1400	600	0.43
Longitudinal Emittance	π mm mrad	1100	2300	2.09
6D emittance	10^{-12} $\times$ $(\pi\ m\ rad)^3$	2000	800	0.40
rms beam size in hydrogen	cm	0.8	0.55	0.69
rms beam size in linac	cm	2.0	1.4	0.70
max beam rad in linac	cm	7.0	7.0	1.0
rms bunch length	cm	1.5	2.2	1.5
max bunch full width	cm	13	19	1.5
rms dp/p	%	3.8	5.6	1.5

This simulation has been confirmed, with minor differences, by the codes double precision GEANT [13] and PARMELA [11].

E. 31 T Solenoid Transverse Cooling Example

As above, the lattice consists of 11 identical 2 m long ‘cells’. The maximum fields are higher (31 T) but the bore smaller (8 cm). The liquid hydrogen absorber is slightly shorter (64 cm long, 6 cm diameter). As before, the direction of the fields in the magnets alternates from one cell to the next. Between the magnets there are again magnetic matching sections (1.3 m long, 32 cm inside diameter) and the rf is also the same (805 MHz, 36 MeV/m).

Table II gives the initial and final parameters for the 31 T example, together with the required emittances for a Higgs factory. In setting these requirements a dilution of 20 % is assumed in each of the three emittances.

TABLE II. Initial and final beam parameters in a 31 T transverse cooling section.

		initial	final	factor	Req.
Particles tracked		4000	3984	99.6%	
Transverse Emittance	π mm mrad	460	240	0.52	240
Longitudinal Emittance	π mm mrad	850	1600	1.9	
6D emittance	$10^{-12} \times (\pi\ m\ rad)^3$	150	95	0.63	98
rms beam size in hydrogen	cm	0.44	0.33	0.75	
rms beam size in linac	cm	1.4	1.1	0.80	
max beam rad in linac	cm	6.0	6.0	1.0	
rms bunch length	cm	1.5	1.8	1.2	
max bunch full width	cm	11	19	1.7	
rms dp/p	%	3.5	5.0	1.4	

F. Bent Solenoid Emittance Exchange Example

The exchange of longitudinal and transverse emittance requires dispersion in a large acceptance channel, followed by low Z wedge absorbers. In this example, the lattice consists of a continuous (3.5 T) solenoid and dispersion is generated by bending the solenoid.

In a bent solenoid, in the absence of any dipole field, there is a drift perpendicular to the bend that is proportional to the particle's momentum. In this lattice, a uniform dipole field is introduced over the bend to exactly cancel this drift for particles with the reference momentum. Particles above and below this reference momentum then drift up or down, depending on their momentum, giving the required dispersion (0.4 m). The dispersion is removed, and the momentum spread reduced, by introducing liquid hydrogen wedges. The hydrogen wedges would be contained by thin beryllium or aluminum foils, but these were not included in this simulation.

After one bend and one set of wedges, the beam is asymmetric in cross section. Symmetry is restored by a following bend and wedge system rotated by 90 degrees with respect to the first. Figure 5 shows a representation of the two bends and wedges. The total solenoid length was 8.5 m. The beam tube outside diameters are 20 cm, and the minimum bend radii 34 cm.

Figure 6(a) shows the magnetic fields (B_z, B_y, and B_x) as a function of the position along the cell. The solenoid bend curvature is exactly that given by the trajectory of a reference particle (equal in momentum to the average momenta given in Fig. 6(b)) in the given transverse fields. It is seen that the onset and end of the bend curvatures is not sudden: the shape is chosen to minimize emittance growth.

The simulations were performed using the program ICOOL [10]. The maximum beam radius is 10 cm. Transmission was 100 %. Figure 7(a) shows the rms longitudinal momentum relative to the reference momentum as a function of the position along the cell. It decreases from an initial value of approximately 5%, to a final value of approximately 2.2%. At the same time, since this is an emittance exchange, the transverse beam area grows, as shown in Fig. 7(b). One notes that the area increases not only in the regions of bends (region 1 and 8), but also in the regions of wedges (2-6 and 9-11). This is probably due to failures in matching that have yet to be understood.

Figure 8 shows scatter plots of the transverse particle positions against their momenta: a) y-p at the start, b) y-p after the first bend c) y-p after the first set of wedges, d) x-p after the first wedges, e) x-p after the second bend, and f) at the end. The dispersion is clearly observed in Fig. 8(b) (after the first bend) and in Fig. 8(e) (after the second). It is seen to be removed, with a corresponding decrease in momentum spread, in Fig. 8(c) (after the first set of wedges) and Fig. 8(f) (after the second set of wedges).

Figure 9 shows a scatterplot of the particle squared radii vs. their longitudinal momentum, Figure 9(a) at the start, and Figure 9(b) at the end. The decrease in momentum spread and rise in beam area are clearly evident.

The initial and final beam parameters are given in Tb. III. The example was not well optimized. There are significant final beam fluctuations, presumably due to mismatching, and some of the 37% rise in 5 dimensional phase space may be from this cause. RF must be included to allow the 6 dimensional emittance to be studied. Significantly more work is needed to further optimize the emittance exchange section.

Emittance exchange in solid LiH wedges, with ideal dispersion and matching, has also been successfully simulated [21] using SIMUCOOL [22]. Dispersion generation by weak focusing spectrometers [20] and dipoles with solenoids [23] have also been studied.

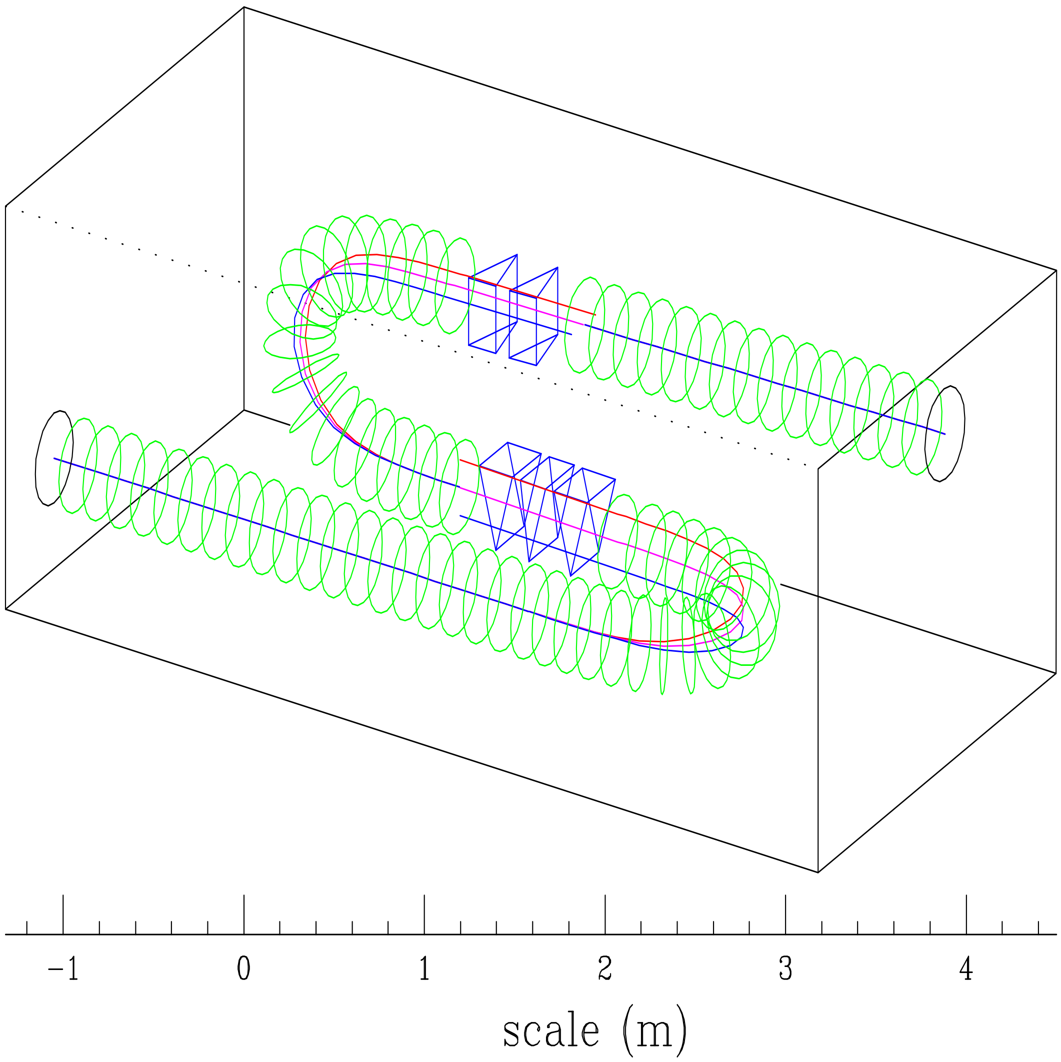

FIG. 5. Representation of a bent solenoid longitudinal emittance exchange section

TABLE III. Initial and final beam parameters in a longitudinal emittance exchange section.

		initial	final	factor
Longitudinal Momentum	MeV/c	9.26	3.35	0.36
Ave. Momentum	MeV/c	180	150	0.83
Transverse size	cm	1.33	2.26	1.70
Transverse Momentum	MeV/c	6.84	7.84	1.15
Transverse Emittance	π mm mrad	870	1694	1.95
$\mathrm{Emit}^2_{trans} \times \mathrm{dp}_{long}$	$(\pi$ m mrad$)^2$ MeV/c	7.0	9.6	1.37

G. RF for the Cooling Systems

RF acceleration sections are used to restore the longitudinal momentum of the muon beam after losses in the cooling media. These rf structures are embedded in solenoidal fields which reverse direction within each section. In the above two above transverse cooling examples, the rf frequency is 805 MHz, the peak gradient 36 MeV/m. The focusing fields, which extend over the cavities, vary from 0 to 5 T, reversing in the center.

In the earlier and later stages, the bunches are longer, and lower frequencies will be required.

In order to realize maximum acceleration gradients within the acceleration cavities, we take advantage of the penetrating properties of a muon beam by placing thin windows between each rf cell, thereby creating an accelerating

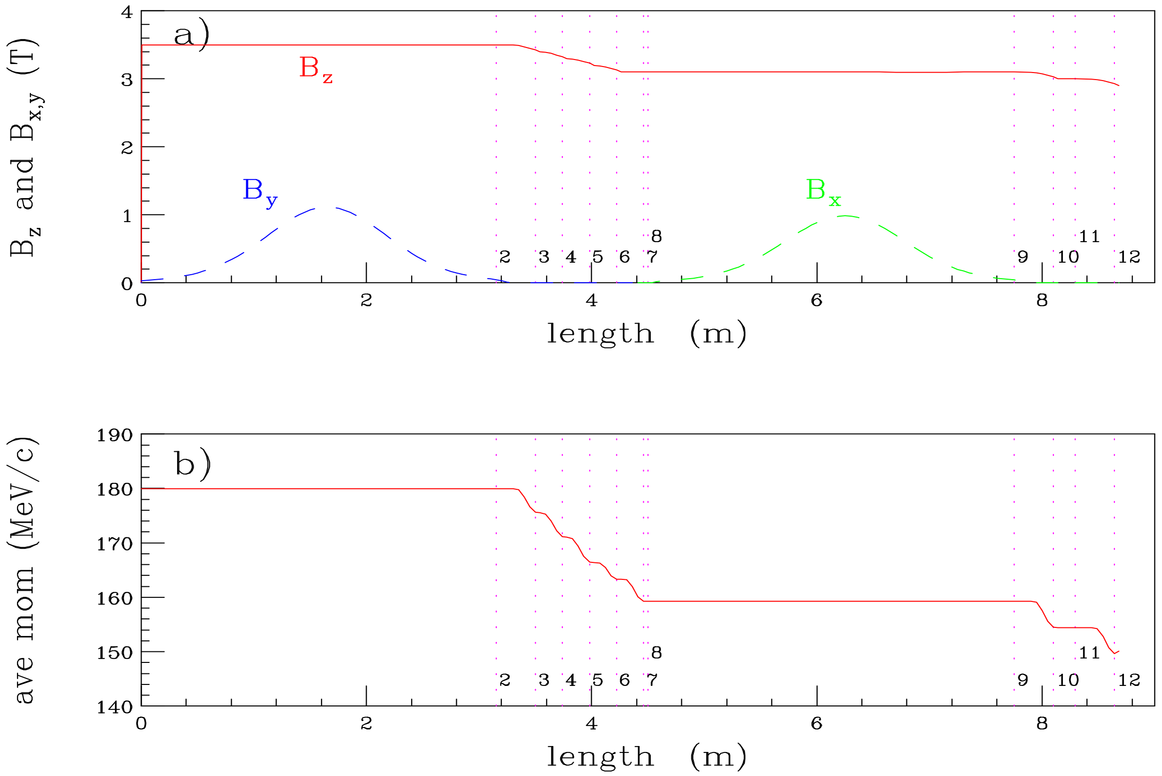

FIG. 6. a) Axial B_z and dipole B_y, B_x, magnetic fields; b) average momentum; both as a function of the position along the cell.

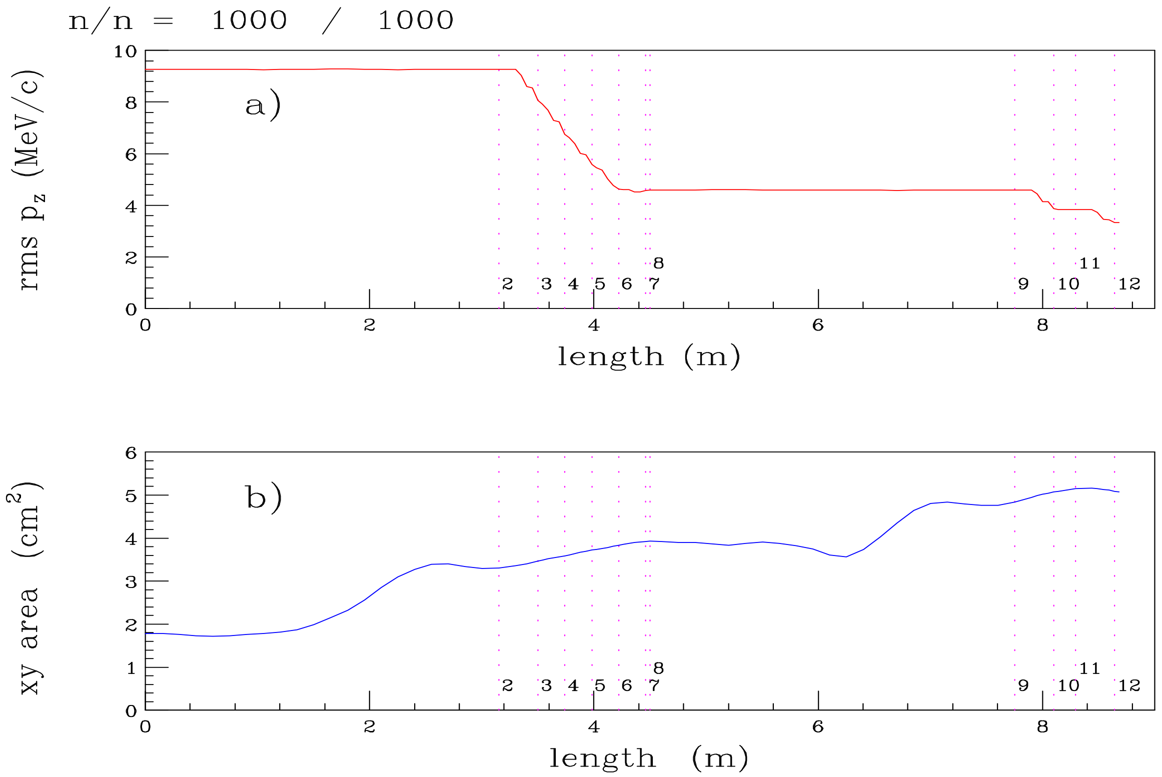

FIG. 7. a) rms longitudinal δp_z with respect to the reference momentum and b) transverse beam area, both as a function of length.

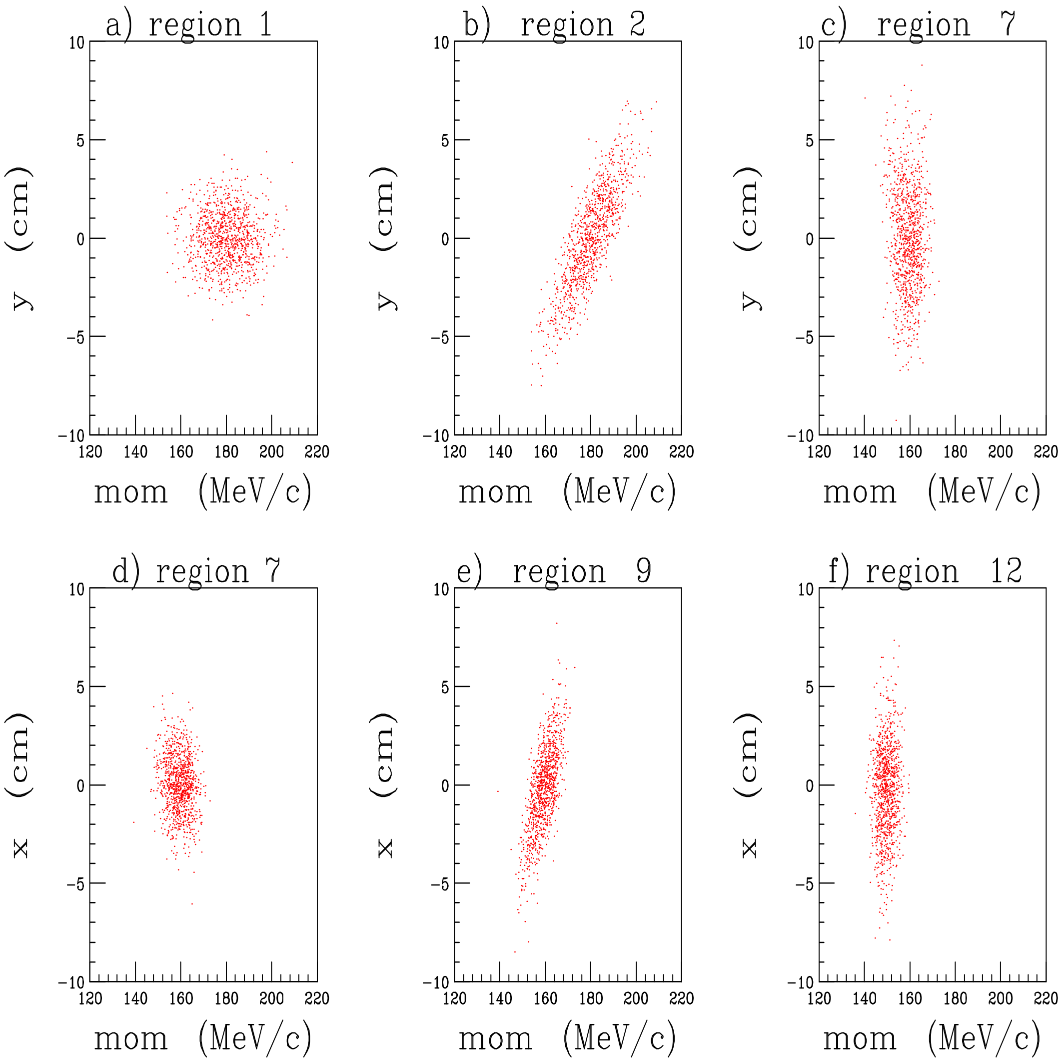

FIG. 8. y-p_z plots: a) at the start, b) after the first bend, c) after the first set of wedges. x-p_z plots: d) after the first wedges, e) after the second bend, and f) at the end

structure closely approximating the classic pill-box cavity. This permits operating conditions in which the axial accelerating field is equal to the maximum wall field and gives a high shunt impedance.

The Be foils in the 15 T example are 16 cm diameter, 125 μm thick Be windows. In the 31 T case, they are 10 cm diameter and 50 μm thick.

For these rf structures, we will use an interleaved cavity design in which two parts are independently powered (Fig. 10). The mode of the system will be referred to as $\pi/2$ interleaved. Each section supports a standing wave π mode, with each acceleration cell $\pi/2$ long, giving a good transit time factor. To reduce the peak rf power requirements (by a factor of 2) the cells may be operated at liquid nitrogen temperatures.

The characteristics of the rf systems currently being studied are summarized in Table IV. Figure 11 shows a full 1.3 m section with interleaved cavities. Each cell is 7.82 cm in length and the 1.3 m section consists of 16 cells.

H. Ionization Cooling Experiment

A proposal has been written [24], and submitted to the FNAL management, which describes a six-year research and development program to develop the hardware needed for ionization cooling, and demonstrate the feasibility of using the ionization cooling technique to produce cooled beams of positive and negative muons. It is proposed to design and prototype critical sections of the muon ionization cooling channel. These sections would be tested by measuring their performance when exposed to single incoming muons with momenta in the range 100 – 300 MeV/c. The phase-space

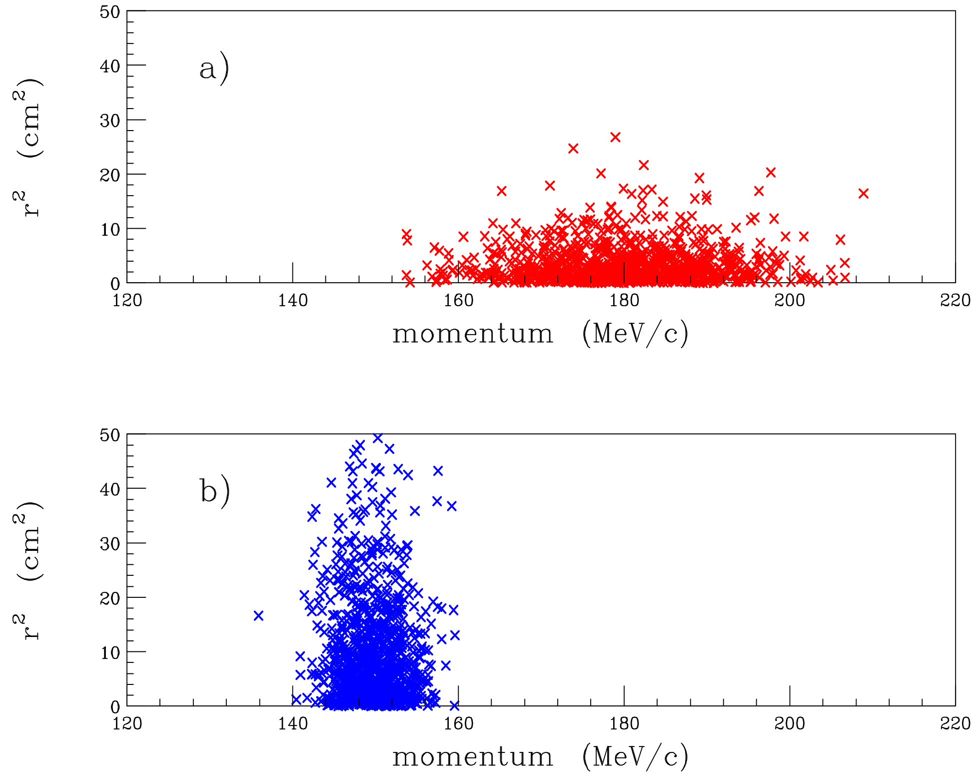

FIG. 9. Scatterplot of squared radii vs. longitudinal momentum a) at the start, and b) at the end.

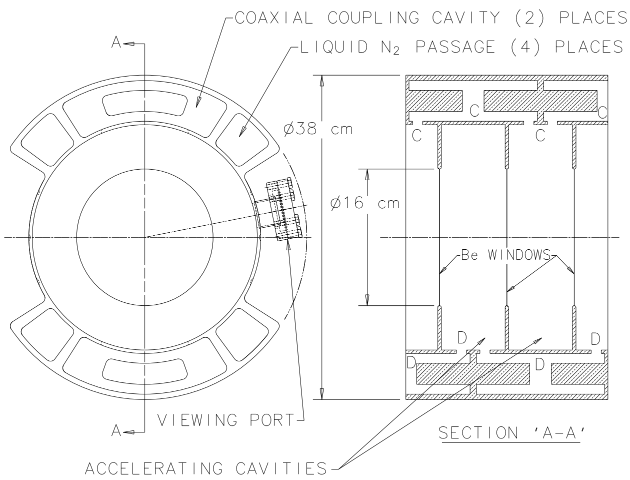

FIG. 10. Two full cell sections plus two half cell sections of the interleaved $\pi/2$ mode accelerating cavities. The volumes labeled **C** are powered separately from the volumes labeled **D**.

volume occupied by the population of muons upstream and downstream of the cooling sections would be measured sufficiently well [25] to enable cooling to be established, the calculations used to design the cooling system to be tested, and optimization of the cooling hardware to be studied. Figure 12 shows a schematic of the detector arrangement to measure the 6-dimensional phase space of the incoming and outgoing muons.

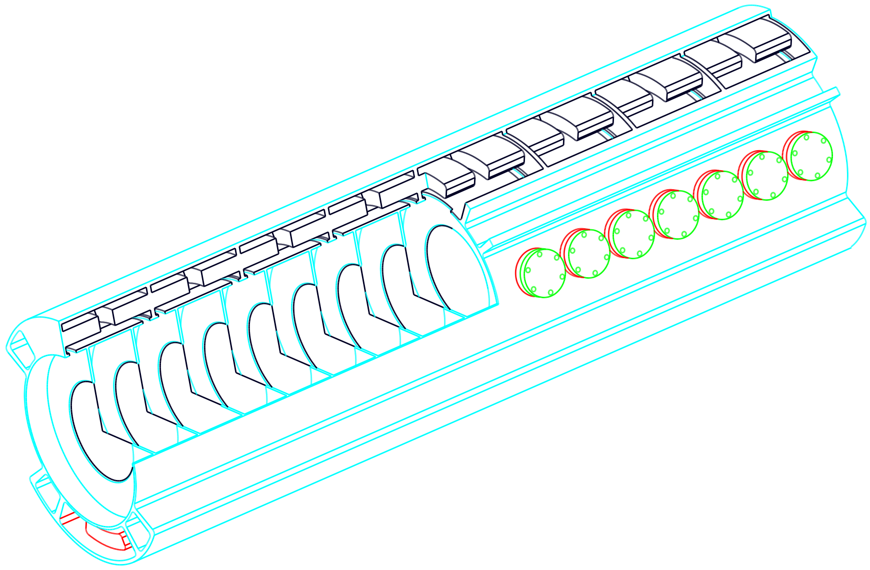

FIG. 11. A 1.3 m acceleration section with quarter section cut away for viewing the inter cavity windows.

TABLE IV. Characteristics of the rf system.

RF Cavity Parameters	
RF frequency [MHz]	805
Cavity Length [cm]	7.82
Cavity Inner Radius [cm]	14.65
Cavity Outer Radius [cm]	19
Q/1000	2 × 20
Peak Axial Gradient [MV/m]	30
Shunt Impedance [MΩ/m]	2 × 54
Zt^2 [MΩ/m]	2 × 44
Fill Time (3 τ) [μs]	26
RF Peak Power [MW/m]	16/2
Ave Power (15Hz) [KW/m]	7/2
Be window aperture [cm]	16 (10 for 31 T case)
Be window thickness [μm]	127 (50 for 31 T case)

[1] A. A. Mikhailichenko and M. S. Zolotorev, Phys. Rev. Lett. **71**, 4146 (1993).
[2] A. Hershcovitch, Technical report, Brookhaven National Laboratory, (unpublished), report BNL-AGS/AD/Tech. Note No. 413.
[3] P. Chen Z. Huang and R. Ruth, in *Proc. Workshop on Advanced Accelerator Concepts*, edited by P. Schoessow (AIP Press, Woodbury, New York, 1995), Vol. 335, p. 646.
[4] A. Bogacz P. Sandler and D. Cline, in *Physics Potential & Development of $\mu^+\mu^-$ Colliders 2^{nd} Workshop*, edited by D. Cline (AIP Press, Woodbury, New York, 1995), Vol. 352, p. 146.
[5] Initial speculations on ionization cooling have been variously attributed to G. O'Neill and/or G. Budker see D. Neuffer in [?].
[6] D. Neuffer, in *Advanced Accelerator Concepts* (AIP Press, Woodbury, New York, 1987), Vol. 156, p. 201, see also [?,?,?].
[7] R. C. Fernow and J. C. Gallardo, Phys. Rev **E52**, 1039 (1995).
[8] R. B. Palmer (unpublished).
[9] A. Van Ginneken, Nucl. Instr. Meth **A 362**, (1995).
[10] R. Fernow, ICOOL, Fortran program to simulate muon ionization cooling.
[11] H. Kirk, Parmela modeling of alternating solenoids, presented at the Mini-Workshop on Cooling BNL, 1998, (unpublished).
[12] *GEANT manual, v.3.2.1, CERN program Library W5013*, CERN, 1994.
[13] P. Le Brun, Alternate solenoid in DPGeant, presented at the Mini-Workshop on Cooling, BNL, 1998, (unpublished).
[14] G. Silvestrov, Proceedings of the Muon Collider Workshop, February 22, 1993, Los Alamos National Laboratory Report

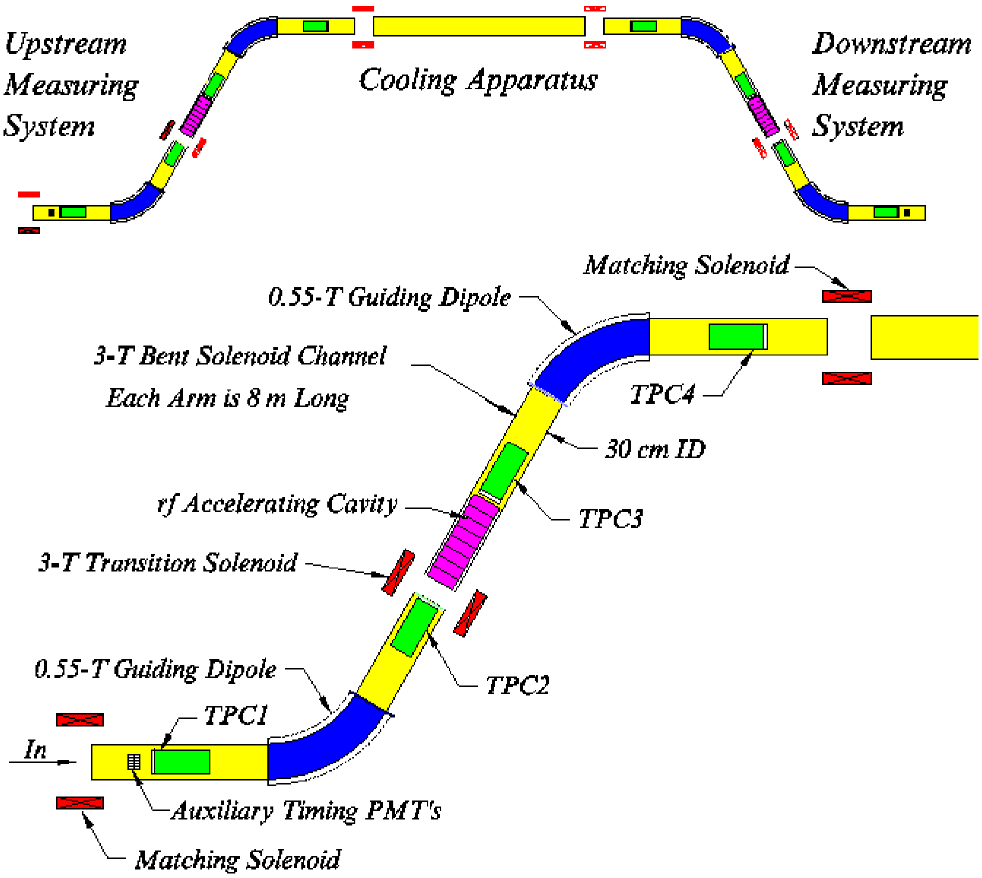

FIG. 12. Schematic of the cooling test apparatus arrangement.

LA-UR-93-866 (1993), (unpublished).

[15] B. Bayanov et al., Nucl. Inst. and Meth. **190**, 9 (1981).

[16] C. D. Johnson, Hyperfine Interactions **44**, 21 (1988).

[17] M.'D. Church and J. P. Marriner, Annu. Rev. Nucl. Sci. **43**, 253 (1993).

[18] G. Silvestrov, in *Proceedings of the 9th Advanced ICFA Beam Dynamics Workshop*, edited by J. C. Gallardo (AIP Press, Woodbury, New York, 1996), Vol. 372.

[19] D. Neuffer, 1979.

[20] V. Balbekov and A. Van Ginneken, presented at the Mini-Workshop on Cooling, Fermilab Oct. 1997 (unpublished).

[21] D. Neuffer, 1979.

[22] D. Neuffer and A. Van Ginneken, presented at the Mini-Workshop on Cooling, BNL Jan. 1998 (unpublished).

[23] D. Neuffer and W. Wan, COSY transport for μ cooling, presentation at the Mini-Workshop on Cooling, FNAL, 1997, (unpublished).

[24] spokesman of the MUCOOL Collaboration S. Geer, Ionization Cooling Research and Development Program for a High Luminosity Muon Collider, Fnal-P904, 1998, available at the URL http://www.fnal.gov/projects/muoncollider/.

[25] K. T. McDonald C. Lu and E. J. Prebys, *A Detector Scenario for the Muon Cooling Experiment*, Princeton/$\mu\mu$/97-8; http://www.hep.princeton.edu/mumu/mumu-97-8.ps, 1997.

[26] R. B. Palmer A. Sessler and A. Tollestrup, in *Proceedings of the 1996 DPF/DPB Summer Study on High-Energy Physics Snowmass'96,* New Directions for High-Energy Physics (Stanford Linear Accelerator Center, Menlo Park, CA, 1997).

[27] E. P. Wigner, Ann. Math. 194 (1939).